Thermodynamics from three-dimensional many-body fragmentation simulations on a cellular automaton model

A. Lejeune*
Université de Liège, Institut de Physique, B5 Sart-Tilman, B-4000 Liège 1, Belgium

J. Perdang†
Institute of Astronomy, Madingley Road, Cambridge, CB3 OHA, United Kingdom
and Université de Liège, Astrophysique, B5c Sart-Tilman, B-4000 Liège 1, Belgium
(Received 29 March 2004; published 1 October 2004)

The thermal equilibrium of many-body systems subject to finite range interactions is investigated numerically, by means of a multipurpose 3D cellular automaton dynamic model developed by the authors. The numerical experiments, carried out at fixed number of bodies, volume and energy, demonstrate the formation of an equilibrium among 3D aggregates of bodies. The distribution of the aggregates against size obeys a power law of (negative) exponent $\tau \approx 2.2$ (against 1.3 in 2D). Our experiments, indicating that the exponent is insensitive to the precise parameter values and the precise parametrization of the interactions, are consistent with the idea of the existence of a universality class corresponding to the thermal equilibrium. The numerical value for the exponent τ is in agreement with the theoretical thermal equilibrium analyses based on various other approaches, numerical and semianalytical, indicating that the cellular automaton approach provides an adequate methodology to investigate thermal equilibria. In this paper, as an illustration of this method, we refer to the problem of formation of clusters of nucleons in heavy ion collisions of nuclei leading on to fragmentation. The theoretical τ value, however, corresponding to the thermal equilibrium among the aggregation clusters, is 15 percent lower than the empirical value (≈ 2.6), as measured in laboratory nuclear fragmentation experiments induced by collision. There is then only a very approximate correspondence between the experimental and the thermal equilibrium value. On the basis of the results of this paper and of a previous paper of this series, we conjecture that the approximate agreement is due to a partial establishment of a thermodynamic equilibrium during the collision of the nuclei. The thermal equilibrium gives the main contribution to the observed τ value; the deviation from this possibly universal value is largely the consequence of the lack of full thermal equilibrium in actual laboratory experiments. This conjecture is extended to interpret the observed ubiquity of power laws of exponents exceeding 2.2, which refer to the distribution of various types of matter in 3D space.

DOI: 10.1103/PhysRevE.70.046201 PACS number(s): 05.45.−a, 25.70.−z, 45.10.−b

I. INTRODUCTION

In two previous papers [1,2] (hereinafter papers I and II) we have developed a Cellular Automaton (CA) approach for simulating the dynamics and thermodynamics of real interacting N-body systems subject to short-range forces. This technique may be competitive with the currently standard methods in this field, namely Monte Carlo simulations (MC) [3–5], and classical molecular dynamics (CMD) [6–8].

In the present paper we are concerned with the statistical equilibrium of a confined three-dimensional (3D) N-body system, and more particularly with the statistical distribution of aggregates of various sizes which form under thermal equilibrium conditions. With the parametrization of the interaction potential we have adopted, our formalism is essentially capable of simulating a broad variety of thermodynamic equilibrium processes, ranging from equilibria among particles on a nuclear, atomic, or molecular scale (nucleons, clusters of ions or molecules) to equilibria among macroscopic-scale particles. More generally, one may ask whether the thermal equilibrium approach remains applicable, at least qualitatively, to any type of cluster-fragmentation process (including the fragmentation of clusters of ions and molecules [9–15]), and of macroscopic aggregates of matter (balls of gypsum, soap balls, frozen potatoes [16]). Experimentally the following main regularities are observed.

(i) The statistical distribution of the fragments [number of fragments, $N(a)$, against size a] is characterized by a power law, $N(a) \propto a^{-\tau}$.

(ii) For microscopic aggregates of matter (clusters of nucleons, ions or molecules) the numerical value of the exponent is of the order of 2.6. For macroscopic aggregates it is smaller. In particular, in the case of cosmic aggregates of matter (the Salpeter mass law of the distribution of stars in the solar neighborhood), $\tau \approx 2.35$ [17]. This suggest that the power law is a universal characteristic of fragmentation processes. The exact value of the exponent seems to be dependent on the precise conditions under which the fragmentation is taking place.

The CA method we adopt here may be viewed as a schematized version of CMD, based on a fully discretized repre-

*Electronic address: a.lejeune@ulg.ac.be
†Electronic address: jperdang@solar.stanford.edu

sentation of the original continuous real dynamical system S. It operates with (1) a discrete time; (2) it is defined in a finite cellular space, of cubic cells in our case; (3) the cellstates are discrete.

The evolution of the cellstates follows a set of rules which mimic the continuous CMD dynamics.

The cellular space, Z_L^3, has a finite volume V. It contains a finite number A of bodies, hereinafter referred to as the "particles." The number A is fixed in all of our experiments, while the volume V of the cellspace is an adjustable parameter. The location of a particle is specified by the cell it belongs to. Accordingly a particle has an intrinsic positional uncertainty in the coordinates, $\Delta x = \Delta y = \Delta z$, fixed by the cellsize λ.

A cell is identified by a triplet of integers playing the parts of coordinates, $\mathbf{r}$. The state of cell $\mathbf{r}$ at time t (integer) is defined by an integer state variable $s(t,\mathbf{r})$ which in our case encodes the dynamic properties (velocity states) of the particles contained in cell $\mathbf{r}$. The state of the CA at time t, $\Sigma(t)$, is the collection of all state variables at time t,

$$\Sigma(t) = \{s(t,\mathbf{r}) | \mathbf{r} \in Z_L^3\}. \tag{1}$$

The global state at time t, $\Sigma(t)$, encodes the full information on the system S under investigation that is accessible from our CA representation.

The state variable of cell $\mathbf{r}$ changes from $s(t,\mathbf{r})$ at time t, to $s(t+1,\mathbf{r})$ at time $t+1$, in response to the interactions of the particles in cell $\mathbf{r}$ with the remaining particles in the system at time step t. We assume that the particle interactions have a finite range. Accordingly we associate with any cell $\mathbf{r}$ an "interaction neighborhood," $N_{\text{int}}(\mathbf{r})$, which is understood as the collection of cells $\mathbf{r}'$ surrounding and containing cell $\mathbf{r}$, such that a particle in the center cell $\mathbf{r}$ interacts exclusively with the particles of this neighborhood. The evolution rule for cellstate $s(t,\mathbf{r})$ then becomes a function of the cellstates $s(t,\mathbf{r}')$ of the interaction neighborhood, $\mathbf{r}' \in N_{\text{int}}(\mathbf{r})$.

In paper II the initial state for our numerical experiments was prepared to simulate faithfully the precollision state of two clusters of actual laboratory experiments. In the illustrative 2D paper I the initial state was a statistically uniform high density cluster of particles. The numerical investigation of the present paper differs from our previous approaches in so far that our initial state is generated by distributing a collection of A particles with uniform probability density over the cells of the finite available lattice space. The initial total kinetic energy is statistically uniformly distributed over the particles; the velocity distribution of the individual particles is statistically isotropic. It seems likely that the initial state defined by this protocol is close to a statistical equilibrium state.

In a collision context (collision of two nuclei, or clusters of ions; collision of a macroscopic aggregate of matter with an obstacle, etc.), this initial state may be roughly compared with the state of a compound cluster which is formed subsequently to the impact of the colliding bodies. Whether efficient energy sharing and eventual equipartition of the energy can be achieved is a matter of the period of confinement of the compound cluster, t_{conf}. Only if the latter exceeds the average collision time between particles, t_{coll},

$$t_{\text{conf}} \gg t_{\text{coll}}, \tag{2}$$

can efficient energy sharing take place. The attractive feature of a thermodynamic calculation is that it is not predicated on a specific and unique physical process responsible for producing the energy and particle exchange among the assembly of aggregates. It is irrelevant whether this mechanism is a collision among two (and possibly more) large initial aggregates, or a collision of one large aggregate with some obstacle, or any other mechanism capable of transferring macroscopic energy to the many microscopic degrees of freedom, which is then shared among the individual degrees of freedom. The final outcome is a thermal equilibrium state which is independent of the precise origin of the input of the energy involved in the exchange processes, and which thereby acquires a certain "universality." Certain broad features of the equilibrium state are shared by any system S of a "universality class" of systems, in our case the 3D many-particle systems with finite range interactions.

In view of these observations it seems to us that a thermodynamic treatment should be an attractive approach to be attempted when dealing with an N-body system S in which *any* mechanism consistent with energy and particle exchange is operating. In general, though, we do not know a priori whether inequality (2), which ultimately legitimizes the thermodynamic treatment, is satisfied for the particular system S we are investigating. This lack of information should not deter us from applying thermodynamics. We are indeed entitled to conceive of an ideal system S^* which is our theoretical equilibrium simulation of a given real laboratory N-body system S. If a discrepancy is detected between the ideal model results of S^* (simulated thermodynamic equilibrium) and the actual observed laboratory results on the real system S (observed features of an experiment dealing with aggregates), then it is imputable to a failure of the idealization S^*, i.e., a failure in the establishment of statistical equilibrium conditions [a violation of inequality (2)]. A variety of laboratory systems S in which physically distinct aggregationlike phenomena manifest themselves, spanning a broad spectrum of linear scales, being characterized by a similar behavior [cf. (i) and (ii) above], we have reasons to surmise that all of these systems can be simulated, at least approximatively, by an idealization of type S^*.

As in paper II, we select the parameters of our modelization S^* to conform to the particular situation of a nuclear fragmentation problem. Our particles are nucleons; the compound cluster is a compound nucleus.

Our CA model remains essentially classical (like the traditional CMD treatment); it does incorporate though several quantum effects.

(1a) The CA lattice imposes an uncertainty in the positions, λ, and in the velocities (or the momenta), v (computational Heisenberg principle of the CA treatment).

(1b) The CA particles are indiscernible and treated as fermions (computational Pauli exclusion principle of the CA treatment).

(1c) Particle-particle scattering is dealt with quantum-mechanically. These effects were included in the treatment of papers I and II.

(2) In the evaluation of the energy of a configuration of nucleons, the quantum-mechanical zero-point energy of the system is schematically taken into account. The latter effect was not considered in papers I and II.

We understand by a "cluster of size a" essentially a geometrically connected collection of nonempty cells containing a particles. The connection of the cells may be achieved facewise, edgewise or vertexwise. With this convention, the geometric connection is in line with the energy connection adopted in this paper. For the precise definition we adopt for a cluster on a cubic lattice space we refer to paper II.

The present paper is a direct extension to 3D of the fictitious 2D thermodynamic equilibrium treatment of a gas of nucleons of paper I. Our objective is to inquire whether the thermodynamic context is pertinent for analyzing real laboratory fragmentation processes of intermediate-size nuclei. To this end we construct from our numerical simulation S^* (a) the frequency of the fragments of size a, $N(a)$, at various densities n and temperatures T (or energies per particle); and (b) the caloric curve.

Our main conclusion is that a complete thermodynamic equilibrium is not realized in actual nuclear fragmentation problems (or other fragmentation problems resulting from collisions, such as molecular cluster fragmentation, etc.). The fully satisfying treatment of those processes requires a direct dynamical simulation of the details of the collision itself. A CA translation of the latter requirement was worked out by the modelization of paper II, in which a numerical agreement of the theoretical and experimental slope values of the frequency of the fragments was achieved. A brief comparison of the thermodynamic approach with the dynamic approach of paper II clarifies the reasons of the partial failure of the equilibrium assumption. At the same time it also makes it clear that the thermodynamic treatment is due to be successful at least to some extent. We do find, indeed, that the thermodynamic treatment has the virtue of exhibiting the following features of the distribution of fragments:

(i) In the thermodynamic equilibrium the distribution can be approximated by a power law, in the range of smaller sizes a; at higher sizes a curvature is observed in a $\log N - \log a$ plot (together with a cutoff, resulting from the finite number of particles).

(ii) At a given density, the slope of the $\log N - \log a$ plot is relatively insensitive to the precise value of the energy, over an intermediate density range from 1/5 to 1/2 the standard nuclear density.

(iii) Numerical evidence suggests that there is a critical density n_c close to 1/3 the standard nuclear density, at which a percolation or aggregationlike phase transition takes place.

II. COMMENTS ON THE 3D CA MODEL

The CA representation we adopt is similar to the representation of the 3D paper II. The lattice space, Z_L^3, is cubic, of dimensionless linear size L, containing L^3 cells. A cell is referred to by a triplet of integer dimensionless coordinates, $(x,y,z)=\mathbf{r}$, measured along the three mutually orthogonal lattice directions $\mathbf{e}_j$ (unit vector along lattice axis $j=1, 2, 3$). The cellular space is assumed to have toroidal topology. This latter assumption means that our CA context actually constitutes a geometric frame for an analysis of infinitely extended matter (infinite nuclear matter in the specific case to be examined by our numerical experiments). In this geometric context Z_L^3 appears as a crystal cell which is repeated indefinitely by translation in the three lattice directions $\mathbf{e}_j$.

In the setup of paper II we followed the collisional energy sharing, and therefore the lattice space was chosen much larger than the size of the colliding clusters. In the present analysis the lattice universe Z_L^3 reduces to the space occupied by the compound cluster. The physical orders of magnitude of the size of an individual lattice cell, λ, and of the time step, $\Delta\tau$, are chosen to conform to the specific nuclear fragmentation problem:

$$\lambda = 1.80 \text{ fm}, \quad \Delta\tau \sim 10^{-23} \text{ s}.$$

This value for λ (slightly lower than in paper II) has been chosen to be consistent under conditions of close packing, both with the radius-mass relation for stable nuclei, and with the average energy per nucleon in stable nuclei (to be discussed below). The volume of the cellspace Z_L^3 is $V=(L\lambda)^3$. An optimal value for the computational parameter $\Delta\tau$ is reestimated at every time step within our CA dynamics. It is found to depend on the density and energy. As an instance, consider the traditional nuclear density $n_o=0.15$ nucleons fm^{-3}, which is realized in our CA setup when we distribute the 300 nucleons over the smallest square lattice, in a way as to have at most one nucleon per cell (lattice size $L=7$; 43 empty cells). We then find an average time step $\langle\Delta\tau\rangle=4.88$, 4.51×10^{-23} s at the energies 16.8, 21.7 MeV per nucleon; the corresponding standard deviation are 0.979, 0.665 $\times10^{-23}$ s.

An instance of the time behavior of the instantaneous step $\Delta\tau$ is given by Fig. 1(a), while Fig. 1(b) exhibits the systematic trend in the energy dependence of the average step. In all cases we have examined, the average step is larger, and exhibits higher fluctuations at the lower energies, while at high energies we have a lower and more stable step.

An individual CA particle a is allowed to exist in one among 7 dynamic states (quantum effect 1a): (i) in a rest state, with velocity $\mathbf{v}_a=0$; (ii) in a moving state, $\mathbf{v}_a=+v\mathbf{e}_j$ or $-v\mathbf{e}_j$, $j=1,2,3$. The allowed nonzero speed obeys $v=\lambda/\Delta\tau$. The state of cell $\mathbf{r}$ at time step t, $s(t,\mathbf{r})$, incorporating the standard CA exclusion principle [quantum effect (1b)], is directly encoded in a 7-bit binary integer. With this choice the highest local density we can simulate is 7 particles per cell, $n_{\max}\approx0.944$ nucleons fm^{-3}. This value is over 6 times as large as the standard density of nuclear matter, $n_o\approx0.15$ nucleons fm^{-3}.

As in paper II, to treat the interactions among the nucleons, we associate an interaction neighborhood with any cell $\mathbf{r}$, $N_{\text{int}}(\mathbf{r})$, which is made of the "central" cell $\mathbf{r}$, the $\varphi=6$ cells having common faces with the central cell; the $\epsilon=12$ cells having common edges, but no common faces; and the $\nu=8$ cells having common vertices with cell $\mathbf{r}$, but no com-

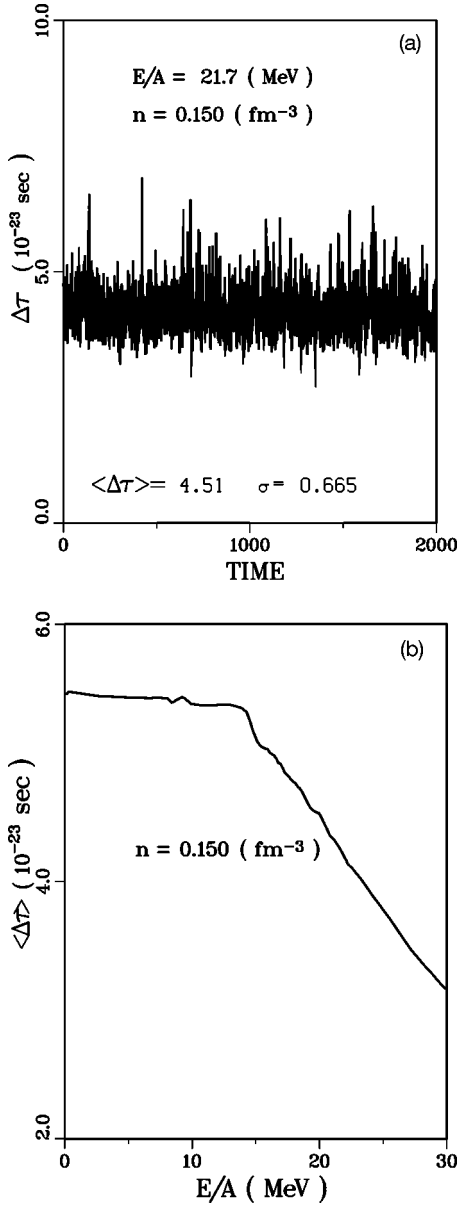

FIG. 1. (a) Evolution of $\Delta\tau(t)$ for a high-density configuration (n_o=0.15 nucleons fm^{-3}), at energy per nucleon E/A=21.7 MeV, over 2000 time steps. (b) Dependence of $\langle\Delta\tau\rangle$ on energy E/A.

mon faces or edges. When listing these neighbor cells, due account is to be taken of the toroidal topology. We point out that our interactions are short-range interactions only; the Coulomb interaction is not explicitly dealt with.

In principle, the interaction potential between pairs of particles in cells $\mathbf{r}$ and $\mathbf{r}'$ is parametrized by 5 coefficients: V_o, ΔV, V_ϕ, V_e, V_v.

(i) If $\mathbf{r}'=\mathbf{r}$ (pair of particles in same cell), then the interaction potential is set equal to V_o (first pair in same cell); $V_o+\Delta V$ (second pair); $V_o+2\Delta V$ (third pair); etc.

(ii) If $\mathbf{r}'\neq\mathbf{r}$ and $\mathbf{r}'\in N_{\rm int}(\mathbf{r})$, then the interaction potential is V_ϕ, V_e, or V_v respectively, depending on whether the cells are face-, edge-, or vertex-joined.

(iii) If $\mathbf{r}'\neq\mathbf{r}$ and $\mathbf{r}'\notin N_{\rm int}(\mathbf{r})$, then the interaction potential is zero.

In our numerical experiments we have set the parameters of the interaction potential equal to the following values: $V_o=V_\phi=-15$ MeV; $\Delta V=+6$ MeV; and $V_\epsilon=V_v=-1$ MeV. With these choices, together with the above choice for λ, we reproduce the following.

(1) The right order of the average energy per nucleon in a nucleus, in the case of a compact packing of the nucleons (one nucleon per cell); at the same time we duplicate the realistic sizes of nuclei. A high enough value of the parameter ΔV has been selected to prevent an unrealistic accumulation of nucleons in a single cell; we thereby avoid an actual realization of very high densities in an equilibrium state, and hence nuclear sizes smaller than the empirical sizes of the stable nuclei.

(2) We also model the qualitative and quantitative features of the caloric curve (Sec. III), temperature T against energy per nucleon E/A. Our numerical experiments have indeed established that the pattern of the caloric curve is quite sensitive to the values of the parametrization of the potential energy.

Schematically, over the energy range over which our experiments are performed, 0.3 MeV per nucleon $<E/A<30$ MeV per nucleon, the caloric curve we generate for various parameter values of the potential energy can be interpolated by a simple algebraic expression (cf. paper I). For our purposes the following representation appears as convenient

$$kT = kT_c(n) + [s(n)F_b(E)]\frac{E}{A}, \quad F_b(E) \equiv \frac{E^b}{E^b + E_{\rm tr}(n)^b} \quad (3)$$

(k, Boltzmann constant). This representation is found to accommodate the empirical data as well (cf. Fig. 5). Equation (3) involves, in principle, four free functions of the density.

(i) The function $T_c(n)$, which plays the part of a critical temperature, depends strongly on the main potential energy parameter, $V_o(<0)$. The higher $|V_o|$ is, the higher $T_c(n)$ becomes. We anticipate that T_c is constrained by the empirical data (Fig. 5).

(ii) The asymptotic slope, $s(n)$, of the temperature at high enough energy $[E/A\gg E_{\rm tr}(n)/A]$, turns out to be independent of the parametrization of the potential, and independent of the density as well. In the asymptotic regime, E/A reduces to the classical kinetic energy per particle, so that $s(n)=2/3$.

(iii) The transition energy $E_{\rm tr}(n)$ depends on all parameters of the potential. This coefficient separates two temperature regimes, a high-energy regime in which the temperature increases linearly with energy, $E\gg E_{\rm tr}(n)$, and a regime in which the temperature is practically independent of the energy, $E\ll E_{\rm tr}(n)$.

(iv) The exponent b is found to be insensitive to the parameters of the potential and of density. The simplest choice, $b\approx 1$, gives a reasonable fit for all of our data points.

With the interaction potential being specified, the thermodynamic equilibrium of our idealized system S^* depends on three extensive thermodynamic variables:

The total number of particles, A; this variable is fixed and set equal to 300 in all of our experiments.

The volume V of the lattice space, or, equivalently, the particle density, n.

The total energy E of the system, or, equivalently, the energy per particle, E/A.

Each experimental run is fully specified by the latter two thermodynamic magnitudes.

(1) Given the particle density, in principle, the size parameter L of the lattice space (and the volume of the configuration), is fixed by

$$L = \frac{1}{\lambda}\left(\frac{A}{n}\right)^{1/3}. \tag{4}$$

But in a CA context L is an integer by definition. Relation (4) then plays the part of a constraining relation on the admissible discrete collection of densities. In order to generate a system S^* required to have an approximate density n_{appr}, we proceed in practice as follows.

(a) We compute a corresponding formal size parameter L_{appr} from Eq. (4); generically the latter is noninteger, and hence nonadmissible.

(b) We introduce as a new admissible size parameter the integer L higher than, and closest to L_{appr} (ceiling function of L_{appr}).

(c) Inserting the new size parameter into the equation

$$n = \frac{1}{\lambda^3}\frac{A}{L^3}, \tag{5}$$

we obtain a corresponding admissible density which is close to n_{appr}, and which we adopt in our computations. For L ranging from 5 to 20, we obtain admissible densities in the interval 0.41 to 0.006 nucleons/fm^3.

(2) The energy E is the sum of the following components. (i) The potential energy of the interacting pairs of particles, W. (ii) The classical kinetic energy, K, of the individual particles. And (iii) the quantum-mechanical zero-point energy of the system, E_o. Moreover, (iv) in order to be consistent with the empirical caloric curve, we redefine the zero of the potential energy as corresponding to the minimum of the potential energy (at the given density n). We discuss these energy contributions separately.

(i) Our program computes the potential energy W from the individual pair-interactions. For instance, for a sample of 30 randomly generated compact configurations we obtain an average of $W/A=-63.6$ MeV per nucleon.

(ii) The total kinetic energy K is equal to the elementary kinetic energy of a single particle in a state of motion, $\Delta K = 1/2mv^2$, times the total number of moving particles, A_{m} (integer). We observe that the elementary kinetic energy ΔK is proportional to $(\Delta\tau)^{-2}$, so that it is quite sensitive to the precise value of this computational parameter. In our specific nuclear problem (m, mass of nucleon), if we set the time step equal to 2.5, 5.0, or 7.5×10^{-23} s, then ΔK is 27.0, 6.8, or 3.0 MeV, respectively.

(iii) With the quantum-mechanical zero-point kinetic energy, E_o, resulting from the fermion nature of the nucleons, we associate a corresponding maximum momentum p_{M} by $E_o/A=p_{\mathrm{M}}^2/(2m)$. If g is the degeneracy parameter of a quantum state, then a cell in the phase space, of "volume" h^3 (h, Planck's non-normalized constant), contains g quantum states, which are all occupied in the case of highest density. Hence, in the traditional elementary treatment the total number of occupied states (total number of available particles, A), is given by

$$A = \int \frac{g\ dx\ dy\ dz\ dp_x\ dp_y\ dp_z}{h^3}. \tag{6}$$

Carrying out the integration from $-p_{\mathrm{M}}$ to $+p_{\mathrm{M}}$ in each momentum component, and from 0 to λL in each position component, and introducing the volume V, and then the density, n, identified with the standard nuclear density n_o, we finally find for the quantum-mechanical zero-point energy per particle

$$\frac{E_o}{A} = \frac{h^2}{g^{2/3}8m}n^{2/3}. \tag{7}$$

Since our treatment deals with a single species of nucleons (no isotopic spin degeneracy), and since it does not explicitly take account of a spin of the nucleons either, we set the degeneracy factor g equal to 1. We then have $E_o/A = 9.33\ 10^{-5}$ ergs=58 MeV. The more detailed calculation leads to the value 53 MeV. The binding energy per nucleon estimated in this fashion becomes $B=W/A + E_o/A \approx -10$ MeV per nucleon, which is the correct order of magnitude. By treating all nucleons as indiscernible–all nucleons are of a single electrically neutral species—we disregard one further energy contribution. As in papers I and II, electrostatic effects are not taken into consideration. The inclusion of the isospin effect would lead to a decrease in the zero-point energy.

The energy per nucleon in our nuclear matter then becomes $W/A+(A_{\mathrm{m}}/A)\Delta K+E_o/A$.

(iv) In the above representation of the interactions, the total potential energy vanishes, $W=0$, when the particles of the system cease to interact. This happens if the density is low enough, so that statistically the interaction neighborhood contains less than one particle. The maximum density consistent with this situation is then 1/27 particle per cell, or $n_{\mathrm{free}} \approx 0.00635$ nucleon fm^{-3}. At densities less than n_{free} the CA model describes an essentially interaction-free ideal gas.

At densities exceeding n_{free}, the potential energy is negative, so that in principle the total energy of the system can become negative as well. To conform to the convention adopted in the representation of the empirical caloric curve of nuclear fragmentation (cf. Fig. 5) in which the zero of the energy is chosen such that the energy is non-negative (and vanishes at $T=0$), we redefine here the zero of our energy scale in the following way.

For a given density, n, denote by $W_{\min}(n)$ the statistical average of the potential energy of the system of particles in the stable thermal equilibrium state, irrespectively of the temperature of the system. If we then shift the potential energy, setting $W^*=W-W_{\min}(n)$, we secure that the latter expression is statistically non-negative. The numerical calculation of $W_{\min}(n)$ is straighforward.

Taking account of (i), (ii), (iii), (iv), we adopt as our final expression for the average energy per nucleon

$$\frac{E}{A} = \frac{A_{\mathrm{m}}}{A}\Delta K + \frac{W}{A} + \frac{E_o}{A} - \frac{W_{\min}(n)}{A}. \tag{8}$$

The assignment of an energy value for our experimental runs proceeds along the following lines. We first observe that the number of moving particles obeys

$$A_{\mathrm{m}} = \frac{E - E_o - W^*}{\Delta K}, \tag{9}$$

which is required to be an integer. Equation (9) plays the role of a constraining relation for the allowed discrete energy spectrum of our CA model.

In practice, we compute an admissible energy value close enough to a trial total energy, E_{appr}, in the following straightforward way. Assume that the (admissible) density n, and hence the required size parameter L have already been obtained.

(a) Distribute the A particles over the available lattice space, Z_L^3, in a statistically uniform way.

(b) Compute the potential energy W corresponding to the spatial configuration of the particles.

(c) Derive a formal number of moving particles, $A_{\mathrm{m\ appr}}$, from Eq. (7). Generically, this number is not an integer.

(d) Substitute to the formal value $A_{\mathrm{m\ appr}}$ the integer A_{m} closest to $A_{\mathrm{m\ appr}}$.

In this paper all total energies E are evaluated by Eq. (8).

III. NUMERICAL EXPERIMENTS AND RESULTS

A. Computation of thermal equilibria

Our experimental investigation has been conducted according to the following protocol.

(1) Suppose that an admissible density n and an admissible total energy E corresponding to our initial tentative values n_{appr} and E_{appr} have been obtained by the procedure discussed in the previous section. In the process, the A particles have been distributed randomly and uniformly over the cellular space Z_L^3 (of size parameter L determined by n). The positional coordinates of all particles are then known. To generate the velocity states of this collection of particles, we choose a subset of A_{m} particles [cf. Eq. (9)] among the full collection of A particles, taking care that this subset is again uniformly distributed over the cellular space. We then assign the 6 nonzero velocity states randomly and isotropically among the subset of A_{m} particles. The remaining $A-A_{\mathrm{m}}$ particles are at rest. This computational step then specifies the initial spatial distribution and the velocity states of the individual particles. Thereby the individual initial cellstates $s(0,\mathbf{r})$, $\mathbf{r} \in Z_L^3$ are known, and hence so is the global initial state $\Sigma(0)$ of the CA.

(2) Given the initial CA state, $\Sigma(0)$, the CA dynamical program as described in papers I and II successively generates a finite sequence of $t_{\max}$ global states,

$$\{\Sigma(1),\Sigma(2),\ldots,\Sigma(t_{\mathrm{trans}}-1),\Sigma(t_{\mathrm{trans}}),\Sigma(t_{\mathrm{trans}}+1),\ldots,\Sigma(t_{\max}-1),\Sigma(t_{\max})\}. \tag{10}$$

For most of our runs we have $t_{\max}=2000$ time steps.

(3) For all initial configurations $\Sigma(0)$ generated according to the above procedure, we observe that the CA system relaxes towards a stable statistical equilibrium after a short transient time t_{trans}. In all cases investigated we have $t_{\mathrm{trans}}<1000$ steps.

In contrast with the methodology of paper I, in which macroscopic magnitudes were computed with respect to single global configurations $\Sigma(t)$ (with $t>t_{\mathrm{trans}}$), we adopt here a procedure which enables us to obtain these magnitudes with a higher precision. Any thermodynamic magnitude Q associated with the statistical equilibrium is obtained by a time-average of the corresponding magnitude $q(t)$ attached with the individual fluctuating global state $\Sigma(t)$, at a time step t, over the equilibrium phase,

$$Q = \langle q \rangle \equiv \frac{1}{t_{\max} - t_{\mathrm{trans}}} \sum_{\theta=1}^{t_{\max}-t_{\mathrm{trans}}} q(t_{\mathrm{trans}} + \theta). \tag{11}$$

Since two successive configurations, $\Sigma(t)$ and $\Sigma(t+1)$, differ little, we single out, in practice, η different times in the equilibrium phase, $t_1, t_2, , \ldots, t_n$, over which the microscopic configuration has changed significantly; we then average over those preselected steps:

$$\langle q \rangle \equiv \frac{1}{\eta}\sum_{j=1}^{\eta} (q(t_j)). \tag{12}$$

For instance, adopting for the temperature the usual classical kinetic definition (energy per kinetic degree of freedom equal to $\frac{1}{2}kT$ in the statistical equilibrium state), we have

$$\frac{3}{2}kT = \Delta K\left\langle \frac{A_{\mathrm{m}}}{A} \right\rangle \equiv \Delta K \frac{1}{t_{\max} - t_{\mathrm{trans}}} \sum_{\theta=1}^{t_{\max}-t_{\mathrm{trans}}} \frac{A_{\mathrm{m}}(t_{\mathrm{trans}} + \theta)}{A}, \tag{13}$$

or

$$= \Delta K \frac{1}{\eta}\sum_{j=1}^{\eta} \left(\frac{A_{\mathrm{m}}(t_j)}{A} \right). \tag{14}$$

B. Equilibrium tests

Several tests were made to assess the establishment of the statistical equilibrium. Figure 1(a) illustrates one of our tests, which displays the fluctuations of the time step $\Delta\tau$ for a high density configuration ($n=n_o$) and a high energy ($E/A=21.7$ MeV), over $t_{\max}=2000$ time steps. In our CA dynamics the computational parameter $\Delta\tau$ is readjusted at each time step to secure rigorous conservation of total energy (cf. papers I and II). During the transient phase this parameter is expected to change systematically, with superimposed statistical fluctuations. Once thermal equilibrium is established, the statistical fluctuations alone survive. The occurrence of these fluctuations is essentially due to the discrete nature of the energy spectrum. If the CA equations of motion require the state of one particle to change from rest to motion with the particle being shifted into a neighbor cell, then the change in total potential energy, ΔW, typically differs from

the change in total kinetic energy, ΔK (elementary kinetic energy of a moving particle). Generically, if ΔA particles change their state of motion and their position, the sum of changes in the kinetic and potential energies of the particles cannot be compensated exactly. To guarantee strict conservation of the energy, the time step $\Delta\tau$ is rescaled.

Initially we set the step $\Delta\tau$ equal to 1×10^{-23} s. As is seen on Fig. 1(a), $\Delta\tau(t)$ jumps up, to stabilize around 4.5×10^{-23} s, practically in less than 200 steps. We observe that $\Delta\tau(t)$ keeps fluctuating in the statistical equilibrium state, around the mean, 4.5×10^{-23} s, with a standard deviation of 0.67×10^{-23} s.

In comparison with traditional statistical mechanics, the number of particles involved in our specific nuclear simulations, $A=300$, is extremely small, so that large relative statistical fluctuations in any extensive magnitude G, $\delta G/G \sim A^{-1/2}(\sim0.06)$, are to be expected in the thermal equilibrium state. These fluctuations are in fact observed in a second test, which is based on the computation of the (instantaneous) temperature $T(t)$ of our system of nucleons, in a single global state $\Sigma(t)$ of the equilibrium phase $t>t_{\text{trans}}$. If we compute the average temperature T over the whole accessible equilibrium range, $t\in[t_{\text{trans}}+1,t_{\max}]$, Eq. (11), together with the standard deviation δT computed by a similar expression, then our experiments give $\delta T/T\sim0.05$. This result is in line with the elementary estimate

$$\frac{\delta T}{T}=\frac{\delta A_{\text{m}}}{A_{\text{m}}}\sim\frac{1}{A^{1/2}}. \tag{15}$$

C. The equilibrium configurations

Plate 2 exhibits several stereoscopic views of instantaneous particle configurations $\Sigma(t)$ at several densities, for t a randomly chosen instant of time of the equilibrium phase.

The pair of Fig. 2(a) represent a global high-density CA state, $n=n_o=0.15$ nucleon fm^{-3}, at low temperature, $T=4$ MeV. With a kinetic energy per nucleon lower than the binding energy, we expect that this system is in a configuration essentially similar to the configuration of a standard stable nucleus. In fact, the figure demonstrates that a single cluster, or compact configuration, is observed, whose (instantaneous) surface assumes an irregular shape. It should be obvious that the surface irregularities are caused by the extra kinetic energy available; these irregularities undergo fluctuations in the course of time. A plot of the global state $\Sigma(t')$, with $t'\neq t$, exhibits a different surface, while the compact configuration remains essentially the same (not shown). Figure 2(a) makes it obvious that we are dealing here with a condensed phase, which has properties reminiscent of a liquid.

The two pairs of Fig. 2(b) refer to global instantaneous CA states of low density, $n=0.051$ nucleons fm$^{-3}\approx1/3n_o$, at two different temperatures.

(i) In the lower temperature regime, $T=4$ MeV, we observe a configuration made of one large central cluster surrounded by clusters of small sizes, $a=1,\ 2,\ 3,\ldots$. As is made clear from a plot of a succession of global states (not shown), the smaller clusters evaporate from the central cluster, and recondense again. This process causes the large cluster to have a more fragmented dynamic surface structure than the clusters of the high density regime [Fig. 2(a)].

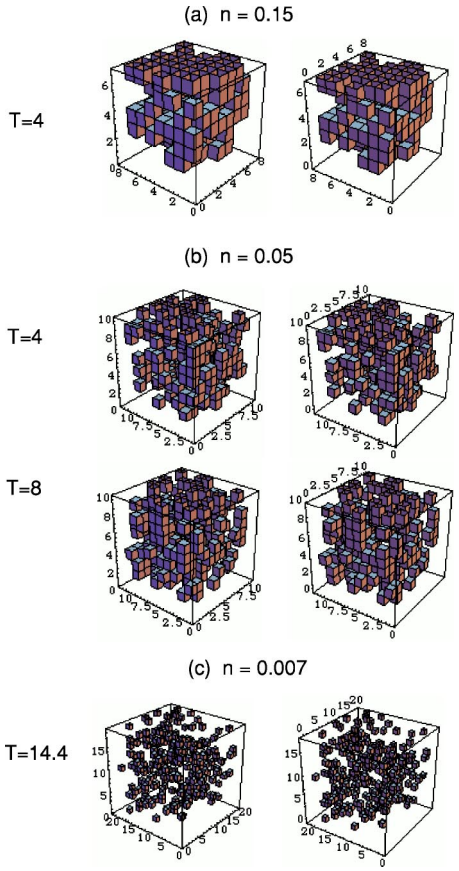

FIG. 2. Stereoscopic views of the spatial configurations (clusters) of nucleons: (a) high density $n=0.15$ nucleons fm^{-3}, low temperature $T=4$ MeV; (b) intermediate density $n=0.051$ nucleons fm^{-3}, (i) low temperature $T=4$ MeV, and higher temperature 8 MeV; (c) very low density $n=0.007$ nucleons fm^{-3}, very high temperature $T=14.4$ MeV.

(ii) In the higher temperature state, $T=8$ MeV, the average kinetic energy per nucleon is of the order of, and slightly higher than the average binding energy, so that the large condensed object at $T=4$ MeV loses its stability. Thereby an equilibrium is established between clusters of different sizes; the configuration is made of clusters of all sizes a (up to the maximum size).

Finally, the pair of Fig. 2(c) illustrate a global state of very low density, close to n_{free}, $n=0.007$ nucleons fm^{-3} $\approx1/21n_o$, and of very high temperature $T=14.4$ MeV. The kinetic energy substantially exceeds the binding energy. It is then manifest that the formation of clusters is energetically not favored. In fact, the configuration we observe is mainly made of clusters of smallest sizes. Under these low density conditions the equilibrium phase is comparable to a gas phase.

To summarize, the plots demonstrate the occurence of a condensed, liquidlike phase at high density (and low temperature) manifesting itself as an essentially single cluster [Fig. 2(a)] and a statistically nearly uniform gaslike phase at low density (and high temperature) presenting itself as a col-

lection of essentially free particles [Fig. 2(c)]. Therefore, one expects a transition between the liquid and the gas phase at some intermediate density. Figure 2(b) is indicative that such a transition manifests itself at some critical density at which clusters of all sizes a are simultaneously present.

D. The cluster distribution

On plate 3 we display the number of clusters $N(a)$ against cluster size $a=1, 2, 3,\ldots$ (number of particles in a cluster), under statistical equilibrium conditions. The plots are shown as usual in log-log form, for a variety of different combinations of densities n and energies per nucleon E/A.

In the first place, it is clear from our results on the spatial equilibrium configurations (plate 2) that two extreme patterns of the cluster distribution are due to occur.

(a) At high densities and low energies, the configuration consists of a single large cluster, generally surrounded by a few clusters of small size; the number of the small clusters decreases rapidly with size [Fig. 2(a)]. Accordingly, the cluster distribution, $\log N(a)-\log a$, consists of (i) a single point at some large a value, the absolute maximum of a, a_{amax} [single cluster, $\log N(a_{\mathrm{amax}})=0$]; (ii) an empty intermediate a range; and (iii) a populated low-a end, $a=1, 2, 3,\ldots,a_{\mathrm{lmax}}$, with the property that $N(a)$ is rapidly decaying with a over the latter interval.

(c) At low densities and high energies, clusters of all sizes up to an absolute maximum size, $a=1, 2,\ldots,a_{\mathrm{amax}}$, appear in the equilibrium distribution [Fig. 2(c)]. The number $N(a)$ decreases again rapidly with size (and is expected to decrease the more rapidly the higher the energy is). The representative points of the cluster distribution are then carried by a curve with a locally negative slope (of absolute value expected to increase with energy).

For these two extreme physical conditions the general nature of the $\log[N(a)]-\log$ (a) distributions is obvious. The corresponding plots are not shown. We only observe that the representative points are nearly linearly distributed over the lower-a range, $a=1, 2, 3,\ldots$. The slopes we find are $\tau_{1-4}\approx 2.1$, under alternative (a) ($n=n_o$; $T=4$ MeV); and $\tau_{1-4}\approx 2.9$ [alternative (c): $n\approx 1/21\ n_o$; $T=14.4$ MeV].

In spite of the qualitative difference in the two extreme spatial configurations, the quantitative slopes of the cluster distribution at the low-a end, τ_{1-4}, remain relatively stable.

We should add that a slope ceases to exist: (i) Under the extreme alternative (a), in the formal limit of zero kinetic energy at high density. We then have just one single cluster left. And (ii) under the extreme alternative (c), in the formal limit of an infinite kinetic energy, at low density. All particles are then free; all clusters are of size $a=1$. (Under the latter alternative we disregard any complications relating to the materialization of other particles, such as pions in the nuclear fragmentation illustration.)

(b) The physically interesting alternative arises in the intermediate density (and energy) range. We have explored more systematically the range $n\approx 1/5$ to $1/2n_o$.

Figures 3 and 4 refer to the distributions of clusters obtained as averages over $\eta=49$ equilibrium configurations $\Sigma(t)$, $t=t_1, t_2,\ldots, t_n$ [Eq. (12)]. Figure 3 exhibits superposed

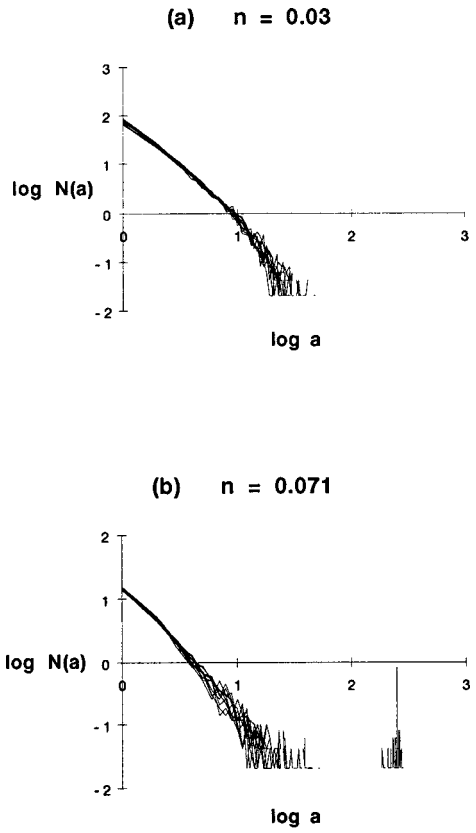

FIG. 3. Superposition of cluster distributions $\log N-\log a$ as measured in the equilibrium state, at fixed density, and at different energies (a) $n=0.030$ nucleons fm^{-3}; $E/A=0.3$, 0.7, 1.3, 1.7, 4.3, 4.7, 6.7, 7.0, 9.3, 9.7, 15.3, 15.7 MeV. (b) $n=0.071$ nucleons fm^{-3}; $E/A=1.0$, 1.3, 5.3, 5.6, 7.6, 8.0, 10.3, 10.6, 16.3, 16.6 MeV.

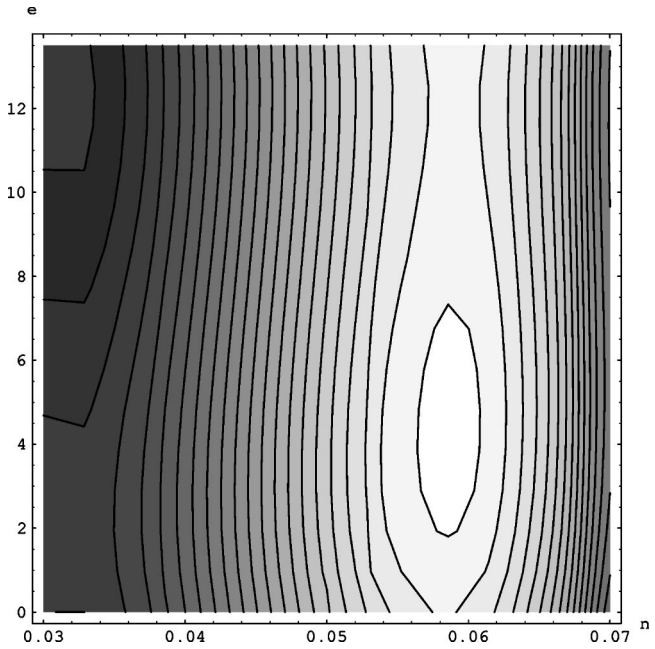

FIG. 4. Size of largest cluster a_{br} shown as a contour plot over the (n, e) plane, $e=E/A$(MeV), n (nucleons fm^{-3}).

$\log N(a) - \log a$ plots for equilibrium configurations at different energies E/A ranging from 0.3 to 16 MeV per nucleon. The densities are 0.030 [panel (a), 12 different energies] and 0.071 [panel (b), 10 different energies] nucleon fm^{-3}. The perhaps unexpected conclusion we are led to draw is that within the precision of our calculations, the curves at fixed density corresponding to different energies (of the range considered) are practically superposable. In other words, at each density level the cluster distribution is only slightly dependent on the energy. The representative points of the $\log N(a) - \log a$ plot trace out a fairly straight line, up to $a \approx 5$. One can notice a clearcut breakoff in the approximate linear distribution at $a = a_{\mathrm{lmax}}$ ($\equiv$ to the absolute maximum, a_{amax}), in the range 28–54 for the lower density $n = 0.030$ nucleon fm^{-3}. And there is a breakoff as well at $a = a_{\mathrm{lmax}}$, in the range $43-103 (\neq a_{\mathrm{amax}} \approx 268-285)$, for the higher density $n = 0.071$ nucleon fm^{-3}. More generally, we have estimated a breakoff for each pair of variables $(n, E/A)$, for which the thermodynamic equilibrium has been investigated, by identifying the characteristic size of the clusters at the breakoff, a_{br}, with a_{lmax}. The latter magnitude is the largest size of the sequence of clusters of sizes $1, 2, \ldots$, whose frequencies $N(a)$ decrease on average with a, and such that a_{lmax} is the highest a value preceding a gap in the distribution of $N(a)$. This leads to an unambiguous specification of a_{br}. We are fully aware, though, that the cluster-size at the breakoff, a_{br}, cannot be determined with high precision. In fact, this parameter is derived from the small number statistics of $N(a)$ (=1 when $a = a_{\mathrm{br}}$), and therefore necessarily subject to large statistical errors. The quantitative conclusions one can draw from the numerical values found for this parameter under different physical conditions are then expected to be subject to large fluctuations as well. Our CA equilibrium calculations are indicative that a_{br} is a well-defined function of density n and energy per particle E/A,

$$a_{\mathrm{br}} = F(n, E/A). \tag{16}$$

More precisely, our results indicate that a_{br} is strongly dependent on the density, and only slightly on the energy. This conclusion is consistent with an observation made above.

To filter out the statistical fluctuations in a_{br} we have approximated the function $F(n, E/A)$ by a polynomial interpolation, $P_k(n, E/A)$, of degree k. Figure 4 is the contour plot of this representation for $k = 3$, in the $(n, E/A)$ plane. The locus of maxima is seen to lie on a nearly vertical critical density line, $n_{\mathrm{br}} \approx 0.058$ nucleon fm^{-3}, or roughly,

$$n_{\mathrm{br}} \approx 1/3 n_o. \tag{17}$$

Due to the small numbers of representative clusters involved in the estimate of a_{br} for a given CA experiment, the probable error in the position of the critical density line is of the order of 25%. We can be confident, however, that statement (17) does hold. The absolute maximum of the polynomial interpolation is at $n = 0.059$ nucleon fm^{-3}, $E_{\mathrm{m}}/A = 4.24$ MeV per nucleon. We should mention that the interpolation produces a surface which is much flatter than the original surface of the direct CA model results, a property which supports our observation that the position of this critical density curve cannot be determined with high precision. There is little doubt, however, that the critical line over which the breaks (and hence the clusters of maximum size) occur, obeys an equation

$$n_{\mathrm{br}} = N(E/A), \tag{18}$$

which is only slightly dependent on E/A (or temperature). Therefore, if a true maximum with respect to E/A exists, the critical value of E/A cannot be ascertained with any confidence. These conclusions are also supported by an interpolation with a polynomial of degree $k = 2$, which locates the critical curve at $n_{\mathrm{br}} \approx 0.052$ nucleon fm^{-3}; there is no maximum with respect to E/A.

Our numerical results are consistent with three alternatives.

In the thermodynamic limit, $(V, A) \to \infty$, with $A/V \to n$, finite, the critical line given by Eq. (17) may correspond to a line of maximimum-size aggregation clusters (a) which are all of infinite size; (b) which remain of finite size except at the point n_{br}, E_{m}/A; or (c) which remain all finite.

Under both alternatives (a) and (b) we have to conclude that the idealized particle system S^* (extrapolated to the thermodynamic limit) undergoes an aggregation-type phase transition. Under alternative (c) the system continuously and smoothly passes from the gas phase to the liquid phase and vice versa, without suffering a phase transition. Our experiments provide a numerical clue suggesting that alternative (c) is to be ruled out. Namely, the largest cluster we encounter at n_{br}, E_{m}/A, extends from one limiting plane of the cellular space to the opposite limiting plane, i.e., it does indeed define an infinite cluster in the crystallographic interpretation of our lattice. Such an experimental property is adopted as the standard computational criterion for an aggregation or percolation phase transition.

The same numerical criterion also suggests that alternative (b) is unlikely to hold. The most probable alternative is then (a). Equation (18) appears as defining a thermodynamic coexistence curve separating a liquidlike phase from a gaslike phase.

As a complementary question, we attempt to characterize analytically the cluster distribution in the neighborhood of the coexistence curve, for densities in the range $n = 0.030$ to 0.071 nucleon fm^{-3}. Our purpose is to represent the $\log N(a) - \log a$ curve by an algebraically simple interpolation formula which (i) is capable of allowing us to estimate a stable (negative) slope value τ (which can then be compared with laboratory slopes of nuclear fragmentation experiments); and which (ii) is capable of duplicating the curvature effect, clearly visible in Fig. 3.

The following parabolic representation:

$$\log N(a) = \nu(a_{\mathrm{ref}}) - \tau(a_{\mathrm{ref}}) \log \frac{a}{a_{\mathrm{ref}}} + \kappa \left(\log \frac{a}{a_{\mathrm{ref}}} \right)^2, \tag{19}$$

complies with these requirements. In this expression a_{ref} is the reference cluster size in the neighborhood of which we wish to estimate a linear slope, $\tau(a_{\mathrm{ref}})$. In particular, if we set $a_{\mathrm{ref}} = 1$, then the coefficient $\nu(1)$ gives the best estimate of the logarithm of the number of free particles (particles of size 1),

log $N(1)$. The coefficient κ provides a measure of the curvature of the representation; this coefficient is independent of the reference size. To switch from reference size 1 to an arbitray reference size a_{ref}, we have the relations

$$\tau(a_{\mathrm{ref}}) = \tau(1) - 2\kappa \log a_{\mathrm{ref}},$$

$$\nu(a_{\mathrm{ref}}) = \nu(1) - \tau(1)\log(a_{\mathrm{ref}}) + \kappa(\log a_{\mathrm{ref}})^2. \qquad (20)$$

Our results indicate that with the choice $a_{\mathrm{ref}}=4$ (average of the a-range considered above), the estimate for the slope $\tau(4)$, becomes practically independent of the density (within the 0.030 to 0,071 nucleon fm^{-3} range) and the energy per nucleon (in the interval 0.3 to 16 MeV)

$$\tau = \tau(4) = 2.23 \pm 0.15, \qquad (21)$$

where the error is here the maximum deviation we have observed over all of our numerical results.

The curvature parameter κ depends on the density n and the energy per nucleon E/A. We have approximated the latter functional dependence by a polynomial of degree k. Our numerical experiments indicate that the linear interpolation relation, $k=1$, which we conveniently write in dimensionless variables

$$\kappa(n,E/A) = \kappa_o + s_n\frac{n}{n_o} + s_E\frac{E/A - B}{B}, \quad \kappa_o = -1.365,$$

$$s_n = +4.67, \quad s_E = -0.19, \qquad (22)$$

gives already an adequate approximation to our CA results ($B=8$ MeV, binding energy per nucleon). Since the sensitivity coefficient to energy, s_E, is small in absolute value as compared to the sensitivity to density, s_n, it is clear that κ depends only marginally on the energy. An interpolation by a polynomial of degree 3, which has been tried as well, does not significantly modify the above results.

The curvature vanishes if

$$\frac{n}{n_o} = \frac{n_c}{n_o} + \epsilon\frac{E/A - B}{B}, \quad \frac{n_c}{n_o} = 0.292, \quad \epsilon = 0.040. \qquad (23)$$

Since the coefficient ϵ is small, the curvature vanishes essentially at a critical density $n_c \approx 0.292\, n_o = 0.044$ nucleon fm$^{-3} \approx 1/3n_o$. The latter result is indicative that the critical curve in the $(n,E/A)$ plane at which κ vanishes is to be identified with the critical curve of maxima of a_{br}, Eq. (17), within the precision of our results.

Since the curvature κ vanishes on the critical curve n_c, an *exact* power law holds

$$N(a) = N(1)a^{-\tau}, \qquad (24)$$

where $\tau \equiv \tau(4) = 2.23$. The exact power law is regarded as the fingerprint of an aggregation-type phase transition.

E. The caloric curve

The CA caloric curve, T against E/A, computed for $E/A > 0.3$ MeV, and with the temperature understood as the kinetic temperature of the nucleons, is displayed in Fig. 5,

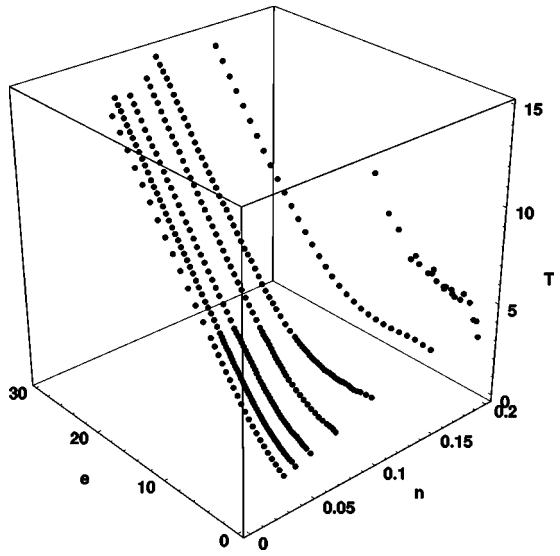

FIG. 5. CA caloric curves, $T-e$ [T, kinetic temperature of nucleons (MeV), $e=E/A$(MeV)] at densities $n=0.15$, 0.10, 0.071, 0.051, 0.039, 0.030 nucleon fm^{-3}. Experimental caloric curve Au-Au fragmentation (shown at fictitious density 0.2 nucleon fm^{-3}).

for the collection of decreasing densities $n=0.15$, 0.10, 0.071, 0.051, 0.039, and 0.030 nucleon fm^{-3}. Instead of estimating the temperature over η states of the thermodynamic equilibrium phase [Eq. (14)], we have computed here the average temperature over η different runs.

In a preliminary experiment, all parameters of the interpolation formula, Eq. (3), were regarded as adjustable parameters. Our curve fitting program indicated that for all densities the best estimates for s and b were close to 0.667 and 1 respectively. The asymptotically linear rising branch corresponds to a perfect gas behavior, so that we should indeed find a slope value $s(n)$ equal to 2/3, independent of density. At the highest densities of the series, $n=0.15$ and 0.10 nucleon fm^{-3}, the reconstructed curve, Eq. (3), deviates qualitatively from the CA result in the low-energy region, in so far as the plateau occurs at a lower temperature level and is shorter. We have therefore not taken account of the CA data at these latter densities in the remaining calculations.

In a second experiment, we set $s=2/3$, and $b=1$ by hand, so that only the two parameters T_c and E_{tr}/A remain to be adjusted. These parameters are found to be well approximated by linear relations in the density, which we can write in dimensionless form

$$\frac{kT_c}{B} = \theta + \sigma_n\frac{n}{n_o}, \quad \theta = 0.148, \quad \sigma_n = 0.194,$$

$$\frac{E_{\mathrm{tr}}/A}{B} = \epsilon' + \sigma_n'\frac{n}{n_o}, \quad \epsilon' = 0.026, \quad \sigma_n' = 2.18. \qquad (25)$$

Practically the coefficient ϵ' is seen to be negligible, so that that the transition energy E_{tr} is just proportional to the density in the lower density range.

Qualitatively the thermodynamic caloric curves we obtain for the 3D nuclear matter are comparable with the caloric

curves of the 2D simulations of paper I. Due to computational difficulties in the low-energy range in the 2D case, it was not manifest how the slope pattern would continue towards the lower energies. In the present 3D simulations our results indicate unambiguously that for $E<E_{\rm tr}$, the curve tends to become *horizontal*. In particular, for the higher densities of 0.15 and 0.10 nucleon fm^{-3} the CA results show the existence of an approximately horizontal extended plateau in the caloric curve at the lower energies. We recall that the caloric curve we construct is a curve at constant available volume V, rather than the traditional caloric curve at constant pressure. Under constant volume, the observed plateau is only approximately horizontal.

In the case of the highest density, this plateau seems to terminate with a bend towards a zero temperature for a small enough energy (Fig. 5). The low energy branch of the curve has not been computed. The high discretization involved in the current version of the CA method does not allow us to handle the particle dynamics at very low kinetic energies. The presence of a plateau is consistent with the occurrence of a phase transition.

This becomes transparent if we regard the caloric curve as an energy-temperature curve (at constant density), and we adopt the analytic approximation [Eq. (3), with $b=1$]. Close enough to the temperature T_c we have, keeping the dominant order in $[T-T_c(n)]$ only

$$\frac{E(T)}{A} \sim \left(\frac{E_{\rm tr}(n)}{A} \frac{3}{2} k[T - T_c(n)] \right)^{1/2}, \quad \text{and}$$

$$c_n(T) \propto (T - T_c)^{(-\alpha)}, \quad \alpha = 1/2, \tag{26}$$

the function $c_n(T)$ representing the specific heat at constant density. The latter magnitude exhibits therefore a singular behavior at the temperature $T_c(n)$. We observe that the numerical value of the critical exponent α depends only on the value of the exponent b describing the transition in the caloric curve of our interpolation formula [Eq. (3)].

It is intuitively clear, and it is manifest from our plots of the spatial configurations (plate 2), that the singularity relates to the formation, or the disruption, of clusters of large (infinite) size, as the temperature is decreased or increased, $\delta T<$ or >0, respectively. Both steps involve indeed huge changes in the energy of the system, $\delta E = c_n \delta T \to \infty$ near T_c. And conversely, near the critical temperature, any amount of energy δE we introduce into the system is used to break the bonds among the nucleons which are bound in the clusters; or any energy we extract from the system leads to the merger of clusters with other clusters of bound nucleons. There is then no change of temperature accompanying the change of energy $\delta T = 1/c_n \delta E \to 0$ near T_c. Such features leave little doubt that at the temperature T_c the system of particles undergoes a genuine phase transition. Quantitatively, the specific heat diverges for a temperature exactly equal to T_c, which is realized for $E/A \equiv 0$ only (within the range of validity of our interpolation formula). Practically however, the temperature T_c is realized, and the specific heat becomes very large, over the full approximately horizontal branch of the caloric curve, i.e., over an extended energy interval, E/A. The size of the latter increases with the density. For instance, at the density of $\approx 1/3 n_o$, the specific heat exceeds 7 times the ideal gas value, at any temperature <7 MeV. At higher densities the curves of high constant specific heat in the $n-E/A$ plane become approximately normal to the density axis (cf. the curves of maxima of $a_{\rm br}$, or of vanishing curvature κ). At low densities the specific heat remains equal to the ideal gas value for nearly any energy E/A, except close to the limit $E/A=0$. Qualitatively, the existence of a critical temperature at which the specific heat becomes large is thus consistent with the indicators of a phase transition discussed above.

F. A brief comparison with empirical data

The laboratory caloric curve in Fig. 5 drawn at a fictitious density ≈ 0.2 nucleon fm^{-3}, corresponds to the NUPECC interpretation of the fragmentation results of an Au-Au collision experiment [8]. The curve exhibits a plateau at the temperature level $T_c \approx 4.5$ MeV, extending from an energy of ≈ 6 MeV per nucleon down to ≈ 2 MeV per nucleon. In the limit of low enough energies the temperature is theoretically required to vanish. This trend is indeed indicated by the experimental data points in the range $E/A<2$ MeV (and suggested by our CA results for the case of the highest density).

We wish to insist that the conditions of our CA model calculations are not identical with those of the laboratory experiment, so that a quantitative comparison of the CA caloric curves with the laboratory data is not meaningful. The small number of model parameters involved in the interaction potential has been adjusted to obtain theoretical curves which are consistent with the general behavior of the experimental data (for $E/A>3$ MeV per nucleon). The laboratory plateau is approximately duplicated for the highest density we investigated, $n=n_o$ (standard nuclear density). Quantitatively the theoretical plateau occurs at a temperature of 4 MeV, which is 11 percent lower than the temperature of the experimental plateau. This difference may be due, at least in part, to the fact that in the ^{197}Au-^{197}Au fragmentation 394 nucleons are involved, against 300 in our numerical setup. Besides, it is manifest that the differences are due, in part also, to the incompleteness of the physics included in our treatment. We recall in particular that the electrostatic interactions, disregarded in our treatment, lead to a contribution of 10 percent to the binding energy. The effect of the Coulomb interaction has been discussed in [25]. Finally, as already pointed out, the thermodynamic equilibrium conditions cannot be fully applicable to the nuclear fragmentation experiments. We come back to this point at the end of this section.

Qualitative similarity and quantitative lack of exact agreement, as observed between the theoretical and the empirical caloric curves, also apply to the theoretical and empirical cluster-size distributions. The CA results indicate that a power law, Eq. (24), holds close to a critical density, Eq. (17), over a broad range of energies per nucleon. The best estimate for the (negative) exponent of the distribution we derive from our CA thermodynamic equilibrium configurations is $\tau_{\rm equ}=2.2$. This value is consistent with the value

derived by other authors adopting different statistical equilibrium models ([21] for a review). Our results indicate that this value is insensitive not only to the precise energy of the many–body configuration, but also to the details of the interactions (the parameter values of the potential energy). This provides numerical evidence for a universality of the observed τ value. The universality class depends (1) on the dimensionality d of space (in 2D, $\tau \approx 1.35$, paper I); this dimensionality effect is well known in critical phenomena. We further conjecture that it may depend also (2) on the precise cluster definition, namely (a) on the cell geometry, and (b) on the allowed mode of connection of the cells. The latter point needs to be substantiated by further experiments.

Qualitatively the laboratory distribution curve of the fragments against size is consistent with a power law (cf. [18–20] for details on the empirical distribution of the fragments resulting from collisions of different nuclei). Quantitatively, the experimental (negative) exponent is $\tau_{\mathrm{exp}} \approx 2.6$. We thus have a relative discrepancy with respect to the empirical value, $(\tau_{\mathrm{exp}} - \tau_{\mathrm{equ}})/\tau_{\mathrm{exp}}$, of 15 percent. Although not totally different from the CA thermodynamic model result, this value is sufficiently higher than the theoretical value, so that the difference is to be regarded as physically significant.

We believe that the approximate agreement, on the one hand, and the relatively minor numerical discrepancies between the statistical models and simulations (including our own CA simulation) and the nuclear fragmentation laboratory experiments on the other hand, are due to an inadequacy in the thermodynamic assumptions on which this class of models rely. As we argued already in paper II, in a laboratory collision between two nuclei there is no evidence of an occurrence of an intermediate phase of long enough duration, following the actual collision and preceding the onset of the fragmentation processes, during which an efficient energy sharing among all of the nucleons of the two colliding nuclei is taking place (via the formation of a compound nucleus). There is no experimental basis for postulating a phase of thermal equilibrium. On the contrary, the CA simulation of the dynamics of the collisions of paper II, which produce a fragment distribution of slope τ_{dyn} consistent with the slope of the laboratory distribution, $\tau_{\mathrm{dyn}} \approx \tau_{\mathrm{exp}}$, supports the view that there is no formation of a proper compound nucleus of long enough lifetime.

The dynamic experiments of paper II rather indicate that the fragment distribution appears as the outcome of the following.

(i) Peripheral groups of particles of the collision site, which acquire a same outward velocity, one, two, …, time steps after the onset of the collision. These groups, or fragments, then leave the collision site, virtually unimpeded by the remainder of the particles. It is then manifest that the first particles being ejected from the collision site cannot be in thermal equilibrium with the remainder of the particles.

(ii) The dynamic collision experiments of paper II also indicate that already at the earliest time steps following the onset of the collision, two fragments, which may be of a larger size, may be ejected along the collision direction; these fragments correspond to two groups of particles belonging to the original two colliding bodies; they have essentially suffered no deflection. By definition, these larger fragments then do not contribute to energy sharing; they are not in thermal equilibrium with the rest of the system.

(iii) At later time steps successively deeper layers of individual particles, and clusters of particles, are ejected from the collision site. The particles involved have remained confined long enough to exchange energy with the rest of the system. In other words these particles have reached a state of approximate thermal equilibrium.

Within this interpretation suggested by the CA dynamics of the collision, the global fragment distribution resulting from laboratory collision experiments cannot be identified with a fragment distribution in a strict thermodynamic equilibrium state realized under exchanges of energy and particles among the clusters (to be ejected as fragments). Accordingly, in real laboratory experiments we observe a distribution which globally deviates from a statistical equilibrium distribution, but which, on the other hand, is not unrelated to the equilibrium distribution. For all those fragments which are ejected from the collision site under conditions (iii), a sufficient number of time steps following the onset of the collision, have achieved a thermal equilibrium.

We are then led to conclude that the observed fragment distribution is to be viewed as a superposition of a thermodynamic *equilibrium distribution* distorted by *nonequilibrium effects*. Significant distortion is naturally expected on the small-size end (individual free particles, two-particle clusters, …) of the distribution, effect (i), and on the large-size end [effect (ii)]. Since a surplus of smallest clusters is produced during the initial stages following the collision, the small-size end is due to be overpopulated with respect to the equilibrium distribution. This mechanism necessarily generates an increase of the τ value characterizing collision experiments, with respect to the equilibrium exponent, or

$$\tau_{\mathrm{equ}} < \tau_{\mathrm{dyn}} \approx \tau_{\mathrm{exp}}. \tag{27}$$

The equilibrium distributions of the present paper (Fig. 3) and the nonequilibrium distributions (Fig. 4 of paper II) are indeed consistent with this inequality. To summarize, in a schematic treatment of the interactions, the thermodynamic (i.e., equilibrium) CA analysis of the fragmentation process leads to an exponent $\tau_{\mathrm{equ}} = 2.2$. The dynamic (nonequilibrium) treatment of the fragmentation mechanism (all other parameters of the formulation of the problem being held constant) of paper II leads to an exponent $\tau_{\mathrm{dyn}} = 2.6$. The latter value is close to the canonical exponent of nuclear fragmentation as reported in the literature.

IV. OUTLOOK

In this paper we have analyzed the statistical equilibrium configurations of a many-body system, following the evolutionary dynamics of the individual particles on a simple 3D CA model, from an initial randomly prepared state to a final state of thermodynamic equilibrium. Although our flexible CA dynamical program is applicable to classical many-body problems of arbitrary nature, the concrete application we have treated in this paper is dealing with a collection of A interacting nucleons (cf. papers I and II). The initial state, a statistically spatially uniform configuration, is specified by

(i) a number of particles $A=300$ (fixed in all of our experiments); (ii) the total (conserved) energy E of the system; and (iii) the volume V accessible to the particles.

The energy and density ranges investigated are: E/A from 0.3 to 30 MeV per nucleon, n from 0.006 nucleon per fm^3 to the standard nuclear density n_o. Plots of the instantaneous spatial configurations of the individual particles in the thermodynamic equilibrium phase, such as those exhibited on plate 2, show that at low particle densities, $n<1/5n_o$, we have a gas of essentially free particles. At high particle densities, $n>1/2n_o$, we observe a condensed state, essentially a single compact cluster, or a liquid drop. These observations hold for the the full energy range investigated.

In the intermediate density range, clusters of all sizes a occur, with frequencies regularly decreasing with a, up to a maximum a_{br}. The cluster distribution obeys an approximation power law up to a_{br}. The maximum size parameter is strongly dependent on n, and slightly modulated by E/A. Numerical evidence suggests that at a critical density $\approx 1/3n_o$ a percolation cluster is formed (formally, a_{br} tends to diverge). This behavior is indicative of an aggregation-type phase transition.

The conclusion of an occurrence of an aggregation-type phase transition is strengthened by a second result. The $\log N(a)-\log a$ plot of the cluster-distribution $N(a)$ exhibits an exact straight line, characterized by a global (negative) slope, τ, which is found to be close to 2.2, at the critical density of the order of $1/3n_o$. In turn, we notice that if we estimate an overall slope $\tau(a_{\mathrm{ref}})$ for the cluster distributions at arbitrary densities, near $a_{\mathrm{ref}}=4$ [cf. Eqs. (19) and (20)], then we recover the critical slope value 2.2. In that sense, to measure the critical slope value, the precise critical density is not required to be realized.

As a third indicator pointing towards a phase transition we have noticed that the specific heat at constant volume diverges at a critical temperature, Eq. (26), with an exponent $\alpha\approx 1/2$. This temperature corresponds in fact to a broad energy range at densities of the order of $1/3n_o$.

The interpretation of the occurence of an exact approximate power law of the fragments, and, in particular, the universality of the latter in nuclear collision-fragmentation and other fragmentation problems involving matter of an arbitrary physical origin, raises several comments. Our 3D simulations of the thermodynamic equilibrium of systems of many-particles, interacting according to a two-body potential given in parametrized form (and whose parametrization is flexible enough to approximate a broad spectrum of interaction potentials exhibiting a finite lower bound), establish unambiguously that these systems develop energetically bound aggregates of particles. The distribution law of the latter follows an approximate power law with a seemingly universal exponent $\tau\approx 2.2$ [cf. Eq. (24), at $a_{ref}=4$] over a broad range of physical conditions. As discussed in this paper, the fact that for many observed distributions of aggregates the exponent is different from the thermodynamic equilibrium value, and in fact higher (≈ 2.6 in nuclear fragmentation problems), can be interpreted as an off-equilibrium effect. In the case of nuclear fragmentation, this point is supported by our CA simulations of the nuclear collision dynamics.

We conjecture therefore that among the variety of observed power laws referring to 3D aggregates of matter, and which are described by exponents

$$\tau=\tau_{\mathrm{equ}}+|\delta\tau|, \quad 0<|\delta\tau|\ll\tau_{\mathrm{equ}}, \tag{28}$$

there is a large subset that can be interpreted in a similar manner. Namely, in a first approximation a thermodynamic equilibrium is responsible for the overall power law, and the contribution τ_{equ} to the exponent. The correction $\delta\tau$ then measures the departure from the equilibrium.

In particular, on the basis of the discussion outlined in this paper, in any collision problem leading on to fragmentation, one expects an overabundance of small clusters. The extra small-size clusters are then responsible for a positive correction $\delta\tau$. For some power laws (distribution law of avalanches, earthquakes, etc.) more specific paradigms are available (for instance, Bak's sandpile model, and related nonequilibrium models [22–24]) which are capable of providing good approximations to the observed exponents. It remains to be seen whether these specific approaches can be subsumed under the umbrella of disturbed thermodynamic equilibria.

ACKNOWLEDGMENTS

The authors would like to thank J. Richert for helpful discussions. J.P. gratefully acknowledges support from the Royal Society–FNRS European Exchange.

[1] A. Lejeune, J. Perdang, and J. Richert, Phys. Rev. E **60**, 2601 (1999).
[2] A. Lejeune, J. Perdang, and J. Richert, Phys. Rev. E **67**, 046214 (2003).
[3] P. Labastie and R. L. Whetten, Phys. Rev. Lett. **65**, 1567 (1990).
[4] A. Hüller, Z. Phys. B: Condens. Matter **93**, 401 (1994).
[5] D. H. E. Gross, Phys. Rep. **279**, 119 (1997).
[6] W. Bauer *et al.*, Phys. Lett. **150B**, 53 (1985).
[7] X. Campi and H. Krivine, Nucl. Phys. A **620**, 46 (1997).
[8] References [5,6] in NUPECC Report, Nuclear Physics in Europe, edtited by J. Vervier *et al.*, 1997, p. 55.
[9] C. Bréchignac *et al.*, J. Chem. Phys. **90**, 3 (1989).
[10] M. Schmidt *et al.*, Phys. Rev. Lett. **79**, 99 (1997).
[11] B. Farizon *et al.*, Int. J. Mass Spectrom. Ion Processes **164**, 225 (1997).
[12] A. Châtelain and J. M. Bonard, in *Proceedings of the Ninth International Symposium on Small Particles and Inorganic Clusters*, edited by A. Châtelain and J. M. Bonard (Springer, Heidelberg, 1999) [Eur. Phys. J. D 9 (1999)].
[13] R. Kusche *et al.*, Eur. Phys. J. D **9**, 1 (1999).
[14] F. Gobet *et al.*, Phys. Rev. Lett. **87**, 203401 (2001).

[15] M. Schmidt *et al.*, Phys. Rev. Lett. **87**, 203402 (2001).
[16] L. Oddershede *et al.*, Phys. Rev. Lett. **71**, 3107 (1993).
[17] J. Scalo, ASP Conf. Ser. **142**, 20 (1998).
[18] R. W. Minich *et al.*, Phys. Lett. **118B**, 458 (1982).
[19] A. D. Panagiotou *et al.*, Phys. Rev. Lett. **52**, 496 (1984).
[20] A. D. Panagiotou, M. W. Curtin, and D. K. Scott, Phys. Rev. C **31**, 55 (1985).
[21] J. Richert and P. Wagner, Phys. Rep. **350**, 1 (2001).
[22] P. Bak, C. Tang, and K. Wiesenfeld, Phys. Rev. Lett. **59**, 381 (1987).
[23] P. Bak and C. Tang, J. Geophys. Res., [Solid Earth Planets] **94**, 15635 (1989).
[24] V. Frette *et al.*, Nature (London) **379**, 49 (1996).
[25] J. M. Carmona, J. Richert, and P. Wagner, Eur. Phys. J. A **11**, 87 (2001).